GSP-based DoA estimation for a multimission radar

Thales C. Raia, Mariana G. Pralon Thomas, Felipe G. Serrenho and José A. Apolinário Jr.

***Abstract*— A multimission radar (MMR) is employed on a wide range of civilian and military missions. The accuracy of the direction of arrival (DoA) estimation of MMR systems is an important issue when locating targets. In this work, a new approach to DoA estimation based on Graph Signal Processing (GSP) is applied to data from a multimission radar. A comparison of the GSP is carried out with classic DoA estimation algorithms, including Delay and Sum, Capon, and Multiple Signal Classification (MUSIC). A short aircraft trajectory is considered as a reference for estimating parameters such as DoA in azimuth, range and radial velocity, both for simulated and real-life signals. DoA in elevation is estimated for simulated data, considering the MMR architecture and target characteristics. Simulation results have shown that the proposed method achieves estimations with competitive accuracy in comparison to classical DoA estimation methods.**

***Keywords*— Graph Signal Processing, Direction of Arrival Estimation, Array Signal Processing, Multimission Radar.**

I. Introduction

In later years, a topic that has received increased attention is the estimation of parameters related to emitters. Within this context, the localization of emitters, especially with respect to the direction of arrival (DoA), has been the focus of research in fields such as RADAR systems for autonomous driving [1], [2], as well as systems for military application and satellite navigation [3], [4], among others. In order to estimate parameters such as DoA, several techniques, especially the ones based on the response of antenna arrays to incoming waves [5], [6], have been exhaustively investigated over the years. We can divide the estimation techniques into three major groups: conventional (such as multilobe amplitude comparison, beamforming [7], and phase interferometry [5]), Maximum Likelihood (ML) [8]–[11], and subspace-based techniques [12]–[16].

This work addresses the use of a recent DoA estimation technique based on Graph Signal Processing (GSP) [17] in a modern Multimission Radar (MMR). The term multimission radar is usually employed to describe a radar system that supports a wide range of missions, including fire support, surveillance (detecting and tracking of aircraft) and air defense. The radar in which this work focuses on employs a proprietary architecture such that the reflected pulses are processed in order to detect targets and calculate parameters such as 3D position (range, azimuth and elevation), and radial velocity, among others.

Thales C. Raia, Department of Defense Engineering, Military Institute of Engineering (IME), Rio de Janeiro–RJ, e-mail: thalesraia82@gmail.com; Mariana G. Pralon Thomas, Radar Group, Army Technological Center (CTEx), Rio de Janeiro–RJ, e-mail: mari_pra@yahoo.com.br; Felipe G. Serrenho, Department of Electrical Engineering, Military Institute of Engineering (IME), Rio de Janeiro–RJ, e-mail: felipe.serrenho@gmail.com; José A. Apolinário Jr., Department of Electrical Engineering, Military Institute of Engineering (IME), Rio de Janeiro–RJ, e-mail: apolin@ime.eb.br.

The contribution of this paper is the evaluation of the performance of a modified GSP-based DoA estimation algorithm in this scenario, where the zenith angle (complement of the elevation angle) is the parameter to be estimated. Herein, the GSP-DoA algorithm uses only a space-domain graph. Other functionalities of the multimission radar signal processing, such as target range and radial velocity, are estimated from real-life signals.

Due to limitations of the experimental measurement campaign employed in this preliminary investigation, the available real data could not be used for vertical DoA estimation. Nevertheless, signals from the MMR were of paramount importance for guaranteeing that simulated data were as close as possible to real-life data. For this work, as seen in the following section, the array geometry of the MMR was simplified to an equivalent (vertical) eight antenna uniform linear array.

Taking into account the reduced schematic of the MMR under investigation, we built a signal simulator to allow a performance analysis of the GSP-based DoA estimator [17]. The simulated signals were linearly modulated in frequency, two chirps, which have a larger spectral variation than those employed before by the GSP-based DoA estimation method, hereafter referred to as GSP-DoA. Simulation results from a typical scenario are presented to compare estimation performance with classical methods [18], such as Delay and Sum, Capon, and MUSIC (MUltiple SIgnal Classification).

The paper is organized as follows. Section II presents the radar signal processing, the simplified structure of the MMR which explains how we obtained the signals from an antenna array used by a multimission radar to estimate the direction of arrival. In Section III, we provide an overview of the main technique employed herein, the GSP-DoA, as well as brief notes on the classical techniques used for performance comparison. Section IV addresses the experimental results and, finally, conclusions are drawn in Section V.

II. Radar Signal Processing

This section is divided into two subsections. The first presents a simplified radar structure, capable of receiving continuous-time radar signals and down-converting it to a digitized (discrete-time) baseband output, as presented in the block diagram given in Fig. 1. The second subsection addresses the signal processing performed in each channel of Fig. 1, in an attempt to improve the process of detection and estimation of the parameters required for target location.

A. Radar Architecture

The antenna architecture of the MMR under investigation consists of a planar array that, on the reception mode, sums the signals received on each of the horizontal sensors, such that an

M-sensor standard uniform linear array (ULA), as depicted in Fig. 1, is considered for the direction-of-arrival estimation of vertical angles. In this figure, we assume that a modulated continuous-time signal $x_m(t) = s(t-\tau_m)e^{-j\Omega_0(t-\tau_m)} + n_m(t)$, with frequency centered in $\Omega_0 = 2\pi f_0$, impinges in each m-th sensor with its respective time delay τ_m. For narrowband signals, $s(t-\tau_m)$ can be approximated by $s(t)$. The signal contains white Gaussian noise, here represented by $n_m(t)$.

A typical linear frequency modulation (LFM) waveform, a chirp usually used in a pulsed radar system, varying its frequency from f_{min} to f_{max}, can be expressed by $s(t) = \cos\left[2\pi(f_{min}t + \frac{\mu t^2}{2})\right]$, $0 \le t \le l$. In the previous expression, $\mu = B/l$ corresponds to the LFM coefficient [19], with $B = f_{max} - f_{min}$ (chirp bandwidth) and l corresponding to the pulse duration.

The first set of filters and local oscillators—represented in a simplified way in Fig. 1 by BPF1, BPF2 and LO—are responsible for reducing the operating frequency of the radar to an intermediate frequency (IF) which will enter the analog-to-digital (A/D) converter, with sampling rate f_s. After digitizing the signal, its discrete-time version is multiplied by a complex exponential ($e^{j\omega_{IF}n}$) which, passing through a low-pass filter, produces the baseband signal. The sampling frequency is then reduced by a convenient decimation factor (20 in our case). The same procedure is replicated on all channels. The time delay on the m-th channel is given by $\tau_m = (m-1)d\cos(\theta)f_s/v_p$, where d is the distance between adjacent sensors, θ is the direction of arrival (DoA) of the signal of interest (SOI), starting to count from zenith, and v_p is the wave propagation speed. The resulting signals, at the output of each channel, are baseband signals $x_m(k) = s(k)e^{-j\Omega_0\tau_m} + n_m(k)$.

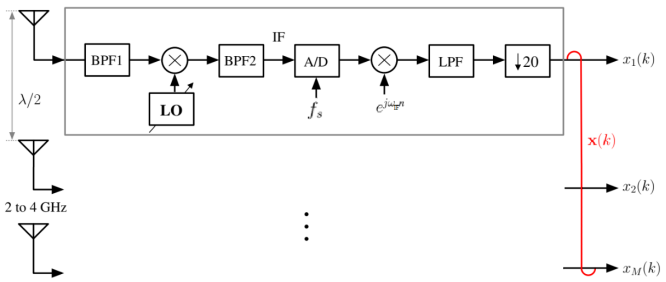

Fig. 1. Multimission Radar (simplified vertical ULA) structure.

B. Signal Processing Functionalities

In order to increase the signal-to-noise ratio (SNR) associated with each pulse in the detection process, the MMR uses a set of filters, per m channel, in the reception. The output signal of the impulse response of the i-th receiving filter (channel index m dropped here for simplicity) may be given by

$$x_{PC_i}(k) = \sum_{\alpha=-\infty}^{\infty} x_i(\alpha)h_i^*(k-\alpha) = x_i(k) * h_i(k), \quad (1)$$

where PC denotes Pulse Compression in each m-th channel and $h_i(k)$ is the i-th filter. After filtering, maximum SNR is attained when the impulse response corresponds to $h_i(k) = s_i(-k)$, i.e., the well known matched filter [19].

At the sample $k = K_0$, representing the exact moment that the i-th reflected pulse from a target arrives at the receiver, we define the signal-to-noise ratio $SNR_i(K_0)$. After pulse compression, the gain in the SNR is known to be

$$G_{PC} = \frac{SNR_{PC_i}(K_0)}{SNR_i(K_0)} = l_{s_i}B_{s_i}, \quad (2)$$

which is referred to as the "Time-Bandwidth Product" [19], l_{s_i} and B_{s_i} corresponding, respectively, to the duration of the pulse and the bandwidth of the i-th transmitted pulse.

SNR improvement is also obtained summing up the reflections of p pulses (complex baseband signals). This procedure is referred to as Coherent Pulse Integration [19]. The output signals of the matched filters, $x_{PC_i}(k)$, $0 < i \le p$, are stored in a buffer and added after receiving the p-th pulse:

$$x_{PI}(k) = \sum_{i=1}^{p} x_{PC_i}(k) = s_{PI}(k) + n_{PI}(k), \quad (3)$$

where PI denotes Pulse Integration in each m-th channel, $s_{PI}(k)$ is the sum of the signal portions and $n_{PI}(k)$ is the sum of the noise portions.

After pulse compression and pulse integration are applied, the range of a single target is obtained from the peak of $x_{PI}(k)$, that is, from instant $T_0 = \max_k |x_{PI}(k)|/f_s$.

Considering that the transmission pulse does not change between transmissions and that the distortion suffered by the p received pulses is time-invariant, it is easy to show that pulse integration results in a SNR gain equal to $G_{PI} = p$. Hence, assuming the same time-bandwidth product for all channels, the overall signal-to-noise ratio gain, after pulse compression and pulse integration, is given as

$$G_{PCPI} = \frac{SNR_{PI}(K_0)}{SNR_i(K_0)} = pB_s l_s. \quad (4)$$

For moving targets with radial velocity, a simple linear summation of pulses may yield wrong results, once a phase variation between reflected signals is observed due to the difference in target range ΔR. To overcome this problem, the MMR applies an FFT in the azimuth direction. This technique consists of a sum with phase correction, where all frequencies in the interval $[\frac{-f_s}{2}, \frac{f_s}{2}]$ are used, with the pulse repetition frequency (PRF) as the sampling frequency. The output signal of the FFT shows a peak in the frequency that corresponds to the target's Doppler frequency (f_D), a peak when the phase has been corrected, representing a coherent integration of the signals. Knowing the Doppler frequency, the radial velocity is obtained by the relation $v_R = \frac{f_D\lambda}{2}$.

We assume, herein, that the azimuth is obtained via a proprietary technique implemented by the MMR which is considered out of the scope of this work. We are interested in estimating the zenith angle (θ), the complement of the elevation angle. The classical DoA estimation problem can be solved from the time delay samples of the M sensors. Our main goal in this paper is to evaluate the performance

of the GSP-based DoA estimation [17] applied to an LMF waveform in an MMR scenario and compare it to classical DoA estimation solutions.

III. GSP-BASED DOA ESTIMATION

In GSP, the object of study is a signal supported on the vertices of a graph. The graph represents complex interactions of the data and, as such, provides a structure that can be exploited. The GSP-Based DoA estimation proposed in [17] uses two directed graphs. The first exploits the spatial information of the array, while the second is based on the time relation about consecutive samples on a single sensor. These graphs are combined via Kronecker product, resulting in a space-time graph. If the DoA is correctly chosen, the Graph Fourier Transform (GFT) tends to have its energy concentrated in one single element. Hence, to estimate the DoA, the GFT-based method performs a grid-search to determine which DoA generates the fittest space-time graph. Nevertheless, in radar applications, although the signal of interest is narrowband in the RF front end, it becomes broadband after being translated to baseband. This makes the use of a time graph unfeasible. As a result, the GSP solution to radar signals adopted herein uses only a space-domain graph (single snapshot estimation). In the following, we provide an overview of the GFT method, giving special treatment to the modifications made to its original version [17].

A. Space-domain graph

In the space-domain graph, each node corresponds to one of the M sensors of the ULA. Distinct space graphs can be proposed. In this work, we connected each node only with its closest neighbors, except for the sensors at the extremities, which are connected with its neighbor and to each other. The weight of each edge is based on the representation of a delay as a multiplication by a complex exponential. When a signal (in the continuous-time domain) is narrowband and analytical, a delay (τ, in second) can be represented by a multiplication by the complex exponential $e^{-j\Omega_0\tau}$, where $\Omega_0 = 2\pi f_0$ is the central frequency of the incoming signal. Although the baseband signal from each antenna is not narrowband, the delay due to a certain DoA is maintained throughout the frequency translation scheme such that the complex exponential is still present in baseband. The proposed space-domain graph can be seen in Fig. 2 while the space-domain adjacency matrix $\mathbf{A}$ is given as:

$$\mathbf{A} = \frac{1}{2}\begin{bmatrix} 0 & e^{j\Omega_0\tau} & 0 & \cdots & e^{j(M-1)\Omega_0\tau} \\ e^{-j\Omega_0\tau} & 0 & e^{j\Omega_0\tau} & \ddots & 0 \\ 0 & e^{-j\Omega_0\tau} & \ddots & \ddots & \vdots \\ \vdots & \ddots & \ddots & 0 & e^{j\Omega_0\tau} \\ e^{-j(M-1)\Omega_0\tau} & 0 & \cdots & e^{-j\Omega_0\tau} & 0 \end{bmatrix},$$

where the division by 2 is so that, defining the snapshot at instant k as vector $\mathbf{x}(k) = [x_1(k) \cdots x_M(k)]^{\mathrm{T}}$, and assuming the input signal a single tone, we can write $\mathbf{x}(k) = \mathbf{A}\mathbf{x}(k)$.

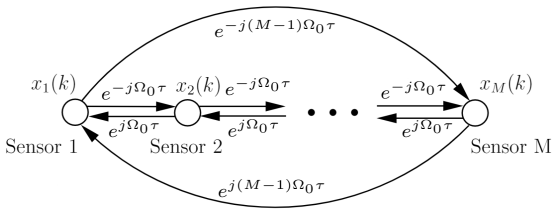

Fig. 2. Space-domain graph.

B. GFT applied to DoA Estimation

The Graph Fourier Transform (GFT) uses the eigenvectors of the adjacency matrix as the frequency components of the transform. Thus, given that the eigendecomposition of the matrix exists, $\mathbf{A}$ can be written as $\mathbf{V}\mathbf{\Lambda}\mathbf{V}^{-1}$, where $\mathbf{V}$ is a matrix formed by eigenvectors and $\mathbf{\Lambda}$ a diagonal matrix with the eigenvalues of $\mathbf{A}$. The GFT of a signal $\mathbf{x}$ is calculated as $\hat{\mathbf{x}} = \mathbf{V}^{-1}\mathbf{x}$ [20]. It is interesting to note that if the adjacency matrix is Hermitian, it is possible to choose a unitary eigenvector matrix $\mathbf{V}$. Doing so, the matrix inversion is simplified to $\mathbf{V}^{-1} = \mathbf{V}^{\mathrm{H}}$ [21].

If the incoming signal is a single tone, vector $\mathbf{x}$ is an eigenvector of $\mathbf{A}$ with unit eigenvalue, as previously noted. Consequently, the elements of the GFT of $\mathbf{x}$ are all zeros, except for the element associated with the eigenvector corresponding to the unitary eigenvalue. Nevertheless, in order for this to happen, matrix $\mathbf{A}$ must be generated considering the correct delays (defined by the DoA) and frequency, which are known since we control the radar emissions. Thus, using correct DoA, the GFT must have its energy mainly concentrated in the GFT element with unitary eigenvalue, while incorrect DoA generates GFTs with more scattered energy.

In order to measure the energy concentration of the GFT, we define an objective function over variable θ, hereinafter referred to as *piquancy function*:

$$\xi(\theta) = \frac{1}{\sqrt{\sum_{i,i\neq i_{\text{eig}}} |\hat{x}_i|^2}}, \tag{5}$$

where i_{eig} is the index of the eigenvector (column of $\mathbf{V}$) associated with the unit eigenvalue; also, $\hat{\mathbf{x}}$ is normalized such that $|\hat{x}_{i_{\text{eig}}}| = 1$.

Defining a grid search, we do not need to compute matrices $\mathbf{A}$, neither perform the decomposition on the fly. Instead, taking into account that $\mathbf{V}$ is a function of θ, but does not depend on the input signal, we can compute and store, in advance, matrix $\mathbf{V}$ for all θ in the grid. This way, the computational cost of each cycle is reduced to the calculation of a matrix-vector multiplication, i.e., $\mathbf{V}^{\mathrm{H}}(\theta)\mathbf{x}$.

Three classic methods of DoA estimation were chosen as the basis for comparison. The first, a non-parametric method known as Delay and Sum beamforming or Barlett aproach [18], estimates the DoA by adding an equal and opposite time delay to each signal in the array. We also used a spectrum-based beamforming, the Minimum Likelihood (ML) beamformer, also known as the Capon beamforming algorithm [22], and MUSIC beamforming algorithm [12]. The MUSIC algorithm uses the spatial covariance matrix

that carries spatial and spectral information of the incoming signals. In all of them, the DoA estimation is carried out through a grid search for the point that generates the output signal with the highest energy.

To estimate the DoA with graph signal processing (GSP) and classical methods, we used signals after pulse compression and pulse integration, as described in the previous section. For all methods, we used a single snapshot, the one with the highest absolute value.

IV. Experimental results

The base scenario for the experiment consists of an aircraft landing trajectory. The experiments were carried out in two different ways: using narrowband signals $x_m(k)$ generated by a simulator, and using data from a real-life MMR. The antenna visibility region in azimuth ranges from $-25°$ to $25°$. The distances between the aircraft and the radar system were obtained from real data and their values are known for the visible region of $3°$ steps. An approach with real signals was carried on. Although real-life *data* were not used to estimate elevation, their use was critical to ensure the correct modeling of the simulated signals in their various nuances. The input elevation angles used in the simulation were based on aircraft altitudes, presented by Flight Radar. Signals were generated as shown in Subsection II-A. Parameters such as range and radial velocity were compared for both simulated and real-life data. The MUSIC algorithm considered the number of signals of interest $D_{SOI} = 2$, the SOI and a clutter.

A. Simulated Radar Signal

A simulation using a sequence of $p = 41$ pulses, with pulse period l and chirp bandwidth B was carried out in the above-described scenario.

To ensure that simulated data were as close as possible to real-life data, the scenario is complemented with clutter and multipath. Clutter has peak power $P_{cl} = \frac{P_{sig}}{2}$, where P_{cl} and P_{sig} are the peak power of the clutter and the received signal, respectively, and signal-to-noise ratio $SNR_{cl} = -21.62$ dB, which represents an object with Radar Cross Section (RCS) of 1 m^2 at 20.01 km. Multipath was implemented considering a Rayleigh Fading Channel, which gives aleatory attenuation and time-delay for each received signal ray. We considered an 8 ray multipath for the signal and a 5 ray multipath for the clutter. Max time-delay for signal multipath is 150 samples, that is, $\frac{3l}{4}$ while max time-delay for the clutter is 100 samples or $\frac{l}{2}$. After coherent pulse integration, the clutter was removed by a 60-point Hann window, centered on the highest energy sample.

The zenith angle estimation was performed with the GSP-DoA and with the classical methods. The same grid was employed for all methods, with a step of $0.001°$. Table I shows the mean absolute error (MAE) of each method. Note that all methods had similar performance, with a slight advantage to the GSP approach. Using range and elevation estimation, we plotted the approximate trajectory in Fig. 3, confirming the feasibility of the system.

TABLE I
Elevation Mean Absolute Error in Degrees

	DS	CAPON	MUSIC	GSP
MAE	$0.0541°$	$0.0541°$	$0.0615°$	$0.0524°$

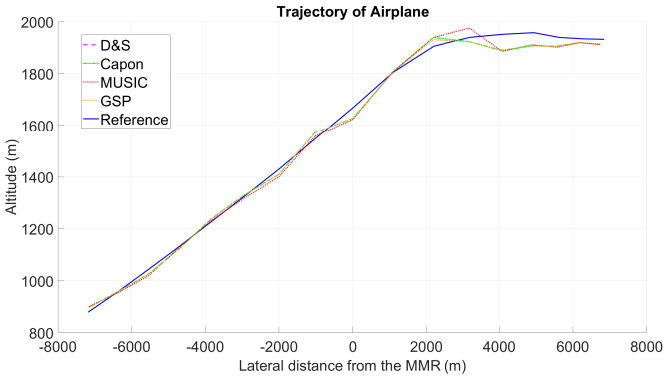

Fig. 3. Estimated target trajectory, x-z view.

The azimuth of $18°$ and its respective target range was chosen arbitrarily as the basis for comparison between simulated and real-life signals. As seen in Subsection II-B, the Time-Bandwidth Product at the instant of interest presents an improvement of the SNR of the order of $SNR_{PC_i} = 10^2 SNR_{x_i}$. After Coherent Pulse Integration an SNR improvement of the order of p times SNR_{PC_i} is achieved, as presented in Fig. 4a. It is clear from this figure the high SNR gain obtained without increasing transmit power.

B. Real Data

The real-life data were collected on August, 27^{th}, 2019, in the vicinity of Viracopos airport, located in the city of Campinas, São Paulo, Brazil.

Data from the MMR signal processing output were used as a reference for the comparison to our estimations. Azimuth and range selected for simulation were, actually, those of the real-life estimations described in this subsection.

For real-life MMR signals, target detection through pulse integration is shown in Fig. 4a. It is in accordance with the simulated signals, the highest peak being located at range 16.645 km; however, several peaks are observed in the vicinity of the peak of interest, probably due to the presence of clutter and multipath due to the vicinity of an urban area. Some techniques as Constant False Alarm Rate (CFAR) [23] can be applied in this situation to improve the probability of detection [18]; however, detection is not within the scope of this work.

Pulse compression and pulse integration agreed with SNR gains achieved in simulation: $SNR_{PC_i} = 10^2 SNR_{x_i}$ and $SNR_{PI} = 41 B_i l_i SNR_{x_i}$, respectively.

A comparison between simulated and real-life data was, also, accomplished for the radial velocity (v_r). For an azimuth of $18°$, real-life radial velocity was 18.42 m/s while the radial velocity estimated from the simulated signal was 18.03 m/s, as shown by the right peaks in Fig. 4b.

The presence of a clutter can, also, be observed in Fig. 4b, where a “no shifted” peak is present in the null radial velocity.

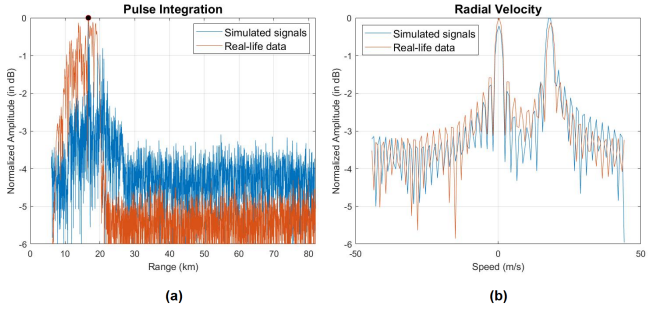

Fig. 4. Simulated and real-life MMR signal processing: (a) Target range observed by using Pulse Integration after compression, and (b) Target Radial Velocity.

The "Azimuth FFT" was applied for all samples along the p compressed pulses.

V. Conclusions

In this paper, we applied the GSP-DoA technique to estimate the elevation angle from simulated signals of a Multimission Radar system. To our understanding, GSP-DoA estimation of linearly modulated frequency (baseband) signals had not been carried out previously. Simulation results show that the proposed method works well for modulated signals, being comparable to classic methods and showing itself as a modern DoA estimation tool. Furthermore, computational complexity can be reduced due to the fact that we can compute offline the eigenvector of the adjacency matrix for each possible DoA. Additionally, a brief comparison between simulation and real *data* suggested, as expected, that techniques applied to enhance the SNR gain tend to increase the probability of the MMR system detecting a target. In a future work, we will focus on the analysis of the processed outputs from the MMR under investigation and perform vertical DoA estimation (zenith angle) of real-data.

References

[1] K. Chang, K. Chen, W. Ma, and Y. Hwang, "An enhanced MUSIC DOA scanning scheme for array radar sensing in autonomous movers," in *2019 IEEE International Conference on Artificial Intelligence Circuits and Systems (AICAS)*, 2019, pp. 152–153.

[2] G. Verma, F. Dagefu, B. M. Sadler, J. Twigg, and J. Fink, "DOA estimation for autonomous systems in complex propagation environments," in *2018 IEEE 19th International Workshop on Signal Processing Advances in Wireless Communications (SPAWC)*, 2018, pp. 1–5.

[3] M. G. Amin, X. Wang, Y. D. Zhang, F. Ahmad, and E. Aboutanios, "Sparse arrays and sampling for interference mitigation and DOA estimation in GNSS," *Proceedings of the IEEE*, vol. 104, no. 6, pp. 1302–1317, 2016.

[4] X. Wang, M. Amin, F. Ahmad, and E. Aboutanios, "Interference DOA estimation and suppression for GNSS receivers using fully augmentable arrays," *IET Radar, Sonar Navigation*, vol. 11, no. 3, pp. 474–480, 2017.

[5] S. V. Schell and W. A. Gardner, "High-resolution direction finding," in *Handbook of Statistics*, N. K. Bose and C. R. Rao, Eds., vol. 10, pp. 757–817. Elsevier Science Publishers, 1993.

[6] S. V. Schell and W. A. Gardner, "Signal-selective high-resolution direction finding in multipath," in *International Conference on Acoustics, Speech, and Signal Processing*, April 1990, pp. 2667–2670 vol.5.

[7] Lei Wang, *Array Signal Processing Algorithms for Beamforming and Direction Finding*, Ph.D. thesis, Department of Electronics, University of York, UK, December 2009.

[8] P. Stoica and A. Nehorai, "MUSIC, maximum likelihood, and Cramer-Rao bound," *IEEE Transactions on Acoustics, Speech, and Signal Processing*, vol. 37, no. 5, pp. 720–741, 1989.

[9] Max Wax, *Detection and Estimation of Superimposed Signals*, Stanford University, Stanford, CA, USA, March 1985.

[10] A. G. Jaffer, "Maximum likelihood direction finding of stochastic sources: a separable solution," in *International Conference on Acoustics, Speech, and Signal Processing (ICASSP)*, April 1988, vol. 5, pp. 2893–2896.

[11] Y. Bresler, "Maximum likelihood estimation of a linearly structured covariance with application to antenna array processing," in *Fourth Annual ASSP Workshop on Spectrum Estimation and Modeling*, August 1988, pp. 172–175.

[12] R. Schmidt, "Multiple emitter location and signal parameter estimation," *IEEE Transactions on Antennas and Propagation*, vol. AP-34, no. 3, pp. 276–280, March 1986.

[13] R. Roy and T. Kailath, "ESPRIT-estimation of signal parameters via rotational invariance techniques," *IEEE Transactions on Acoustics, Speech, and Signal Processing*, vol. 37, no. 7, pp. 984–995, July 1989.

[14] B. Friedlander and A. J. Weiss, "Direction finding using spatial smoothing with interpolated arrays," *IEEE Transactions on Aerospace and Electronic Systems*, vol. 28, no. 2, pp. 574–587, April 1992.

[15] J. Evans, J. Johnson, and D. Sun, "High resolution angular spectrum estimation techniques for terrain scattering analysis and angle of arrival estimation," in *Proceedings of the 1st ASSP Workshop on Spectral Estimation*, McMaster University, Canada, August 1981, pp. 134–139.

[16] Feng-Gang Yan, Zhi-Kun Chen, Ming-Jian Sun, Yi Shen, and Ming Jin, "Two-dimensional direction-of-arrival estimation based on one-dimensional search using rank deficiency principle," *HINDAWI International Journal of Antennas and Propagation*, vol. 2015, pp. 1–8, 2015.

[17] L. A. S. Moreira, A. L. L. Ramos, M. L. R. de Campos, J. A. Apolinário Jr., and F. G. Serrenho, "A graph signal processing approach to direction of arrival estimation," in *27th European Signal Processing Conference (EUSIPCO)*, Sep. 2019, pp. 1–5.

[18] H. L. Van Trees, *Optimum Array Processing: Part IV of Detection, Estimation, and Modulation Theory*, Detection, Estimation, and Modulation Theory. Wiley, 2004.

[19] Bassem R. Mahafza, *Radar Systems Analysis and Design Using MATLAB*, CRC Press, Inc., USA, 1st edition, 2000.

[20] A. Sandryhaila and J. M. F. Moura, "Discrete signal processing on graphs," *IEEE Transactions on Signal Processing*, vol. 61, no. 7, pp. 1644–1656, April 2013.

[21] Lloyd N. Trefethen and David Bau, III, *Numerical Linear Algebra*, SIAM, 1997.

[22] J. Capon, "High-resolution frequency-wavenumber spectrum analysis," *Proceedings of the IEEE*, vol. 57, no. 8, pp. 1408–1418, 1969.

[23] E. Kelly F. Robey, D. Fuhrmann and R. Nitzberg, "A CFAR adaptive matched filter detector," *IEEE Trans. Aerospace Electronic Syst.*, vol. AES-28, no. 28, pp. 208–216, 1992.